© 2018. Published by The Company of Biologists Ltd | Journal of Cell Science (2018) 131, jcs216598. doi:10.1242/jcs.216598

RESEARCH ARTICLE

# ARF6 protects sister chromatid cohesion to ensure the formation of stable kinetochore-microtubule attachments

**Mohamed Bourmoum, Ricardo Charles and Audrey Claing***

## ABSTRACT

Sister chromatid cohesion, facilitated by the cohesin protein complex, is crucial for the establishment of stable bipolar attachments of chromosomes to the spindle microtubules and their faithful segregation. Here, we demonstrate that the GTPase ARF6 prevents the premature loss of sister chromatid cohesion. During mitosis, ARF6-depleted cells normally completed chromosome congression. However, at the metaphase plate, chromosomes failed to establish stable kinetochore-microtubule attachments because of the impaired cohesion at centromeres. As a result, the spindle assembly checkpoint (SAC) was active and cyclin B ubiquitylation and degradation were blocked. Chromosomes and/or chromatids in these cells scattered gradually from the metaphase plate to the two poles of the cell or remained blocked at the metaphase plate for hours. Our study demonstrates that the small GTP-binding protein ARF6 is essential for maintaining centromeric cohesion between sister chromatids, which is necessary for the establishment of stable k-fibres, SAC satisfaction and the onset of anaphase.

**KEY WORDS: ARF6, Cohesion, Mitosis, K-fibres**

## INTRODUCTION

Mitosis ensures the faithful segregation of sister chromatids to daughter cells. Cohesion between sister chromatids is established as early as DNA is replicated during S phase (Uhlmann and Nasmyth, 1998). Upon entry into mitosis, the bulk of the cohesin complex is removed from chromosome arms during the early phases of mitosis, but persists at the centromere until anaphase onset. Cohesin dissolution from chromosome arms during prophase and prometaphase suggests the action of two main mitotic kinases, PLK1 (Sumara et al., 2002) and Aurora B (Giménez-Abián et al., 2004). Centromeric cohesin is, however, sustained and protected by the protein phosphatase PP2A in collaboration with shugoshin until late metaphase (Kitajima et al., 2006). Removal of centromeric cohesin requires satisfaction of the spindle assembly checkpoint (SAC) and is mediated by the protease separase, which cleaves the cohesin subunit Scc1 (also known as Rad21), allowing the separation of sister chromatids and anaphase onset (Waizenegger et al., 2000).

As cells progress from prometaphase to metaphase, chromosomes establish attachments to the spindle microtubules through kinetochores assembled on their centromeres. At early prometaphase, erroneous intermediate attachments are predominant, including lateral (kinetochores are attached to the side wall of microtubules) and monotelic (only one kinetochore of the two is attached to microtubules emanating from one pole) attachments (Godek et al., 2015). Transient lateral attachments play a substantial role in driving chromosome alignment at the spindle equator (Cai et al., 2009). As cells move through mitosis, erroneous attachments are corrected and transformed to end-on, bi-oriented attachments (Shrestha and Draviam, 2013). During this process, Aurora B localizes to the inner centromere and its activity induces error correction by targeting substrates at the outer kinetochore, leading to the destabilization of incorrect kinetochore-microtubule attachments. Bi-orientation creates a centromeric tension and increases the physical distance between Aurora B kinase and its substrates at the outer kinetochore, which stabilizes these attachments (Cimini et al., 2006; Liu et al., 2009). In this context, centromeric cohesion between sister chromatids provides the necessary resistance to the pulling forces of the spindle microtubules, generating the tension needed for the establishment of stable kinetochore-microtubule attachments (Tanaka et al., 2000). The polo-like kinase (PLK1) also contributes to the regulation of these attachments, but its role is more puzzling as its activity can promote both stabilization (Liu et al., 2012) and destabilization (Hood et al., 2012) of microtubules.

When all chromosomes are correctly attached, SAC is satisfied (Musacchio and Salmon, 2007) and the E3 ubiquitin ligase APC/$C^{Cdc20}$ becomes activated, leading to the ubiquitylation and subsequent degradation of cyclin B and securin (Castro et al., 2005). Cyclin B degradation decreases CDK1 activity (Murray et al., 1989) and securin degradation activates separase, allowing the dissolution of sister chromatids (Waizenegger et al., 2000) and the triggering of anaphase. All these processes are tightly controlled and even small misregulation can lead to serious consequences on the cell fate.

Our group has shown that the GTP-binding protein, ADP-ribosylation factor 6 (ARF6) is important for the proliferation of numerous cell types (Bourmoum et al., 2016). This protein is a Ras-like GTPase, and one of the six ARF isoforms identified. ARF6 is localized at the plasma membrane and membranes of the endosomal compartments, where it regulates endocytosis, organization of the actin cytoskeleton and plasma membrane to endosomal traffic (Radhakrishna et al., 1996; Boshans et al., 2000; D'Souza-Schorey et al., 1998). Like all GTPases, it cycles between its GDP- and GTP-bound forms. This cycling is facilitated by guanine nucleotide exchange factors (GEFs) and GTPase-activating proteins (GAPs). ARF6 has been shown to localize to the midbody formed between daughter cells at the end of telophase, where it promotes the completion of cytokinesis through its interaction with mitotic kinesin-like protein 1 (MKLP1) (Makyio et al., 2012). In addition, it was previously proposed that the role of ARF6 in completing cytokinesis is due to its regulation of endosomal to plasma membrane traffic (Schweitzer et al., 2005). In this study, we report that, upstream of cytokinesis, ARF6 plays an important role during the first stages of mitosis. Indeed, this GTPase prevents the precocious loss of sister chromatid cohesion, which is essential for

Department of Pharmacology and Physiology, Faculty of Medicine, Université de Montréal, C.P. 6128 Succursale Centre-ville, Montreal, Quebec, Canada, H3T 1J4.

*Author for correspondence (audrey.claing@umontreal.ca)

A.C., 0000-0002-0742-9083

**Received 7 February 2018; Accepted 25 April 2018**

Journal of Cell Science (2018) 131, jcs216598. doi:10.1242/jcs.216598

stabilization of kinetochore-microtubule attachments, satisfaction of SAC and onset of anaphase.

## RESULTS

### Knockdown of ARF6 delays or blocks cells at mitosis

To elucidate the molecular mechanisms by which ARF6 acts to control proliferation, we first examined the impact of knocking down this GTPase on cell cycle progression. As shown in Fig. 1A, depletion of ARF6 resulted in an 11% increase in the number of cells in $G_2$/M phase and a 12% decrease in cells in $G_0/G_1$ phase without affecting the S phase of the cell cycle. To better understand these findings, we assessed the cell size as well as the proliferation rate of unsynchronized control and ARF6-depleted cells using FACS and cell counting, respectively. We found that the average cell size of ARF6-depleted cells was 15% higher than that in control cells. However, the proliferation rate was strongly reduced (45%) after 2 days of culture in complete medium (Fig. S1). In order to determine precisely in which phase of the cell cycle ($G_2$ or M) ARF6-depleted cells are blocked or delayed, we examined the phosphorylation state of histone H3 (Ser10). The phosphorylation of this mitotic marker was much higher (3.2-fold) in cells infected with ARF6 shRNA lentiviruses than it was in control cells (Fig. 1B) indicating that ARF6-depleted cells were delayed or blocked at mitosis. In these experiments the protein levels of mitotic cyclins (cyclin B and cyclin A) were also assessed. Western blot analysis revealed that cyclin B protein levels were increased by 50% when ARF6 was knocked down. In contrast, cyclin A levels were slightly lower in these conditions (Fig. 1B). To confirm the specificity of ARF6 shRNA, rescue experiments were performed using shRNA-resistant WT-ARF6. As shown in Fig. 1D, overexpression of this construct partially rescued mitotic progression as histone H3 phosphorylation was reduced by 50% in unsynchronized ARF6-depleted cells overexpressing shRNA-resistant WT-ARF6 compared with levels in ARF6-depleted cells transfected with empty vector. To further investigate the role of ARF6 in mitosis, unsynchronized control or ARF6-depleted cells were examined by fluorescence microscopy after labelling DNA with Hoechst 33342. Mitotic cells are easily identified by nuclear envelope breakdown and chromosomes becoming condensed during mitosis. Images were taken (>2400 cells in each condition) and phenotypes of different mitotic stages were scored. Overall, the mitotic index (percentage of total mitotic cells) was 4 times higher in ARF6-depleted cells than in control cells. The frequency of normal mitotic phenotypes including prometaphase, metaphase and anaphase/telophase was similar between control and ARF6-depleted cells. However, we noticed the presence of two abnormal mitotic phenotypes, which were specific to ARF6-depleted cells: (1) a multi-polar spindle phenotype (0.5% of total cells) and (2) the presence of a metaphase plate at the equator with two groups of chromosomes or chromatids positioned symmetrically at the two poles of the cell, which was predominant in ARF6-depleted cells (3% of total cells) and we refer to as the 'prometaphase-like' phenotype. The symmetry of the two groups of chromosomes at the opposite poles of the cell discriminate the prometaphase-like phenotype from the normal prometaphase phenotype in which chromosome positioning is asymmetric (Fig. 1C). In addition, ARF6 depletion heavily increased (10-fold) the number of cells with a bi/multi-lobed nucleus and bi/multi-nucleated cells.

### ARF6 is required for metaphase/anaphase transition

To investigate the origin of the prometaphase-like phenotype observed abundantly in ARF6-depleted cells, we performed live-cell microscopy experiments. Control and ARF6-depleted cells were synchronized at the $G_2$/M border by treatment with the CDK1 inhibitor RO3306. Cells were then released by washing out RO3306 and videos were recorded. Analysis of live cell imaging revealed that chromosome alignment at the spindle equator occurred normally in ARF6-depleted cells, with a delay for a few chromosomes (1-2) in some cells (Fig. 2). In addition, the time taken from nuclear envelope breakdown (NEB) to form the metaphase plate was not affected by ARF6 depletion (59±4.9 min for control cells versus 58±4.5 min for ARF6-depleted cells). However, after forming the metaphase plate, only 49% of ARF6-depleted cells had completed the metaphase/anaphase transition compared with 89% of control cells. Nearly 37% of ARF6-depleted cells that entered mitosis failed to reach anaphase despite successful alignment of chromosomes at the metaphase plate. Chromosomes (or chromatids) in these cells either scattered gradually from the metaphase plate to the two poles of the cell to form the prometaphase-like phenotype or remained blocked at the metaphase plate for hours (Fig. 2A). We also measured the time spent at the metaphase stage in cells that succeeded to enter anaphase and found that ARF6-depleted cells spent twice as much time (26±4.9 min) at the metaphase stage than control cells did (12±1.1 min) (Fig. 2). Even when ARF6-depleted cells succeeded in reaching anaphase and completed mitosis, multiple defects occurred, including lagging chromosomes during anaphase (Fig. S2A) and the formation of a bi- or multi-lobed nucleus in daughter cells after telophase (Fig. S2B). To determine whether the scattered chromosomes observed at the 'prometaphase-like' phenotype are complete chromosomes or separated chromatids, we fixed ARF6-depleted cells 2 h after RO3306 release, labelled centromeres (CENP-A) and examined cells using confocal microscopy. Both single chromatids and complete chromosomes (with two sister chromatids) were found scattered from the metaphase plate to the opposite poles (Fig. S3). Altogether, these results reveal a role for ARF6 during the metaphase/anaphase transition.

### ARF6 depletion blocks degradation of cyclin B but not cyclin A and activates the SAC

Cyclin B degradation is associated with the metaphase/anaphase transition. Since ARF6-depleted cells were blocked at metaphase and failed to enter anaphase, we asked whether cyclin B degradation was affected in these cells. To verify this, control and ARF6-depleted cells were synchronized at the $G_2$/M border (14 h RO3306 treatment), then released by washing out the inhibitor. Cells were lysed and histone H3 phosphorylation, cyclin B and cyclin A protein levels were assessed (Fig. 3A). Control and ARF6-depleted cells entered mitosis similarly after RO3306 release as Histone H3 phosphorylation increased heavily (12-fold) and was comparable between the two conditions 1 h after release. Histone H3 phosphorylation was strongly reduced (75%) in control cells after 2 h from RO3306 release, indicating a rapid mitotic exit, and continued to decrease to very low levels over time. However, in ARF6-depleted cells, phosphorylation of Histone H3 was only mildly reduced (30%) 2 h after release, indicating that these cells remained blocked at mitosis. Histone H3 phosphorylation continued to decrease slowly and remained high even 6 h after RO3306 release. These results are consistent with live cell experiments. Cyclin A and cyclin B levels were at their maximal levels at the $G_2$/M border and were identical between control and ARF6-depleted cells. The time course of cyclin A protein levels revealed that ARF6 depletion did not affect cyclin A degradation. In both conditions, cyclin A protein level was

Journal of Cell Science (2018) 131, jcs216598. doi:10.1242/jcs.216598

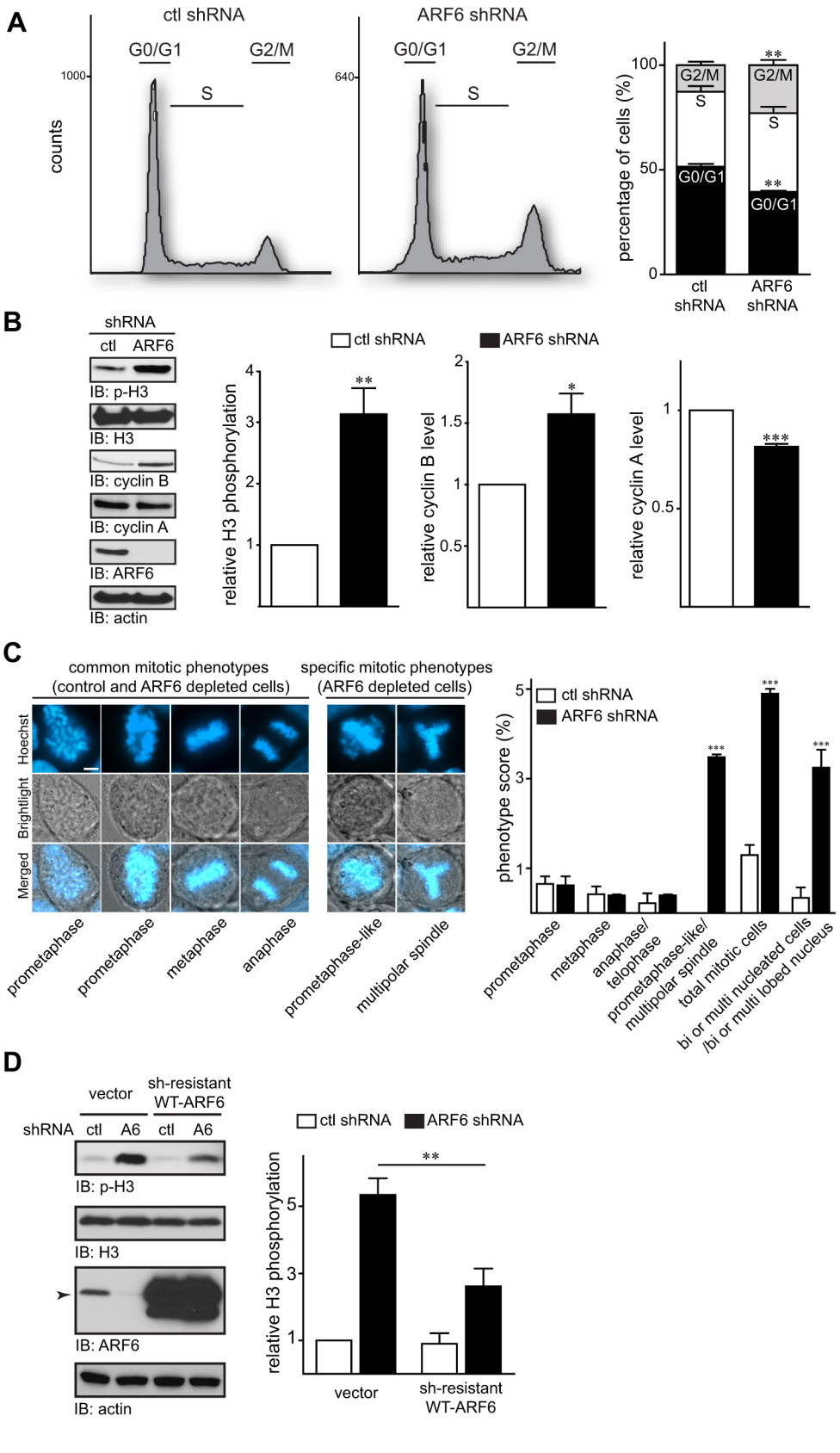


**Fig. 1. ARF6 depletion delays or blocks cells at mitosis.** Unsynchronized control (ctl) and ARF6-depleted cells (day 4 after lentiviral infection) were maintained in complete culture medium. (A) Cells were trypsinized, fixed and subjected to cell cycle analysis using FACS (10,000 events/condition). Quantification of cell populations, in different stages of the cell cycle, was performed using ModFit LT software. The graph shows means±s.e.m. of 4 independent experiments ($n$=4, two-way ANOVA). (B) Cells were lysed and the indicated proteins were assessed by western blot analysis. The graph shows means±s.e.m. of 3 independent experiments ($n$=3, $t$-test). (C) Cells were fixed, DNA was labelled with Hoechst and images were captured with a fluorescence microscope. Scale bar: 5 µm. For quantification, a total of 2418 control cells and 2538 ARF6-depleted cells, from three independent experiments, were analysed. The graph shows means±s.e.m. of 3 independent experiments ($n$=3, two-way ANOVA). (D) Unsynchronized control (ctl) and ARF6-depleted cells (A6) overexpressing or not shRNA-resistant WT-ARF6 were lysed and the indicated proteins were assessed by western blot analysis. The graph shows means±s.e.m. of 4 independent experiments ($n$=4, two-way ANOVA). *$P$<0.05, **$P$<0.01, ***$P$<0.001.

maintained 1 h after release and 35% of this cyclin was degraded after 2 h. After 6 h, 65% of cyclin A was similarly degraded in control and ARF6-depleted cells. In contrast, cyclin B degradation was altered in ARF6-depleted cells. 1 h post RO3306 release, the cyclin B level remained unchanged and similar between control and ARF6-depleted cells. After 2 h, cyclin B was massively degraded (50%) in control cells but remained elevated in ARF6-depleted cells (only a 15% decrease). After 6 h, 87% of cyclin B



Journal of Cell Science

Journal of Cell Science (2018) 131, jcs216598. doi:10.1242/jcs.216598

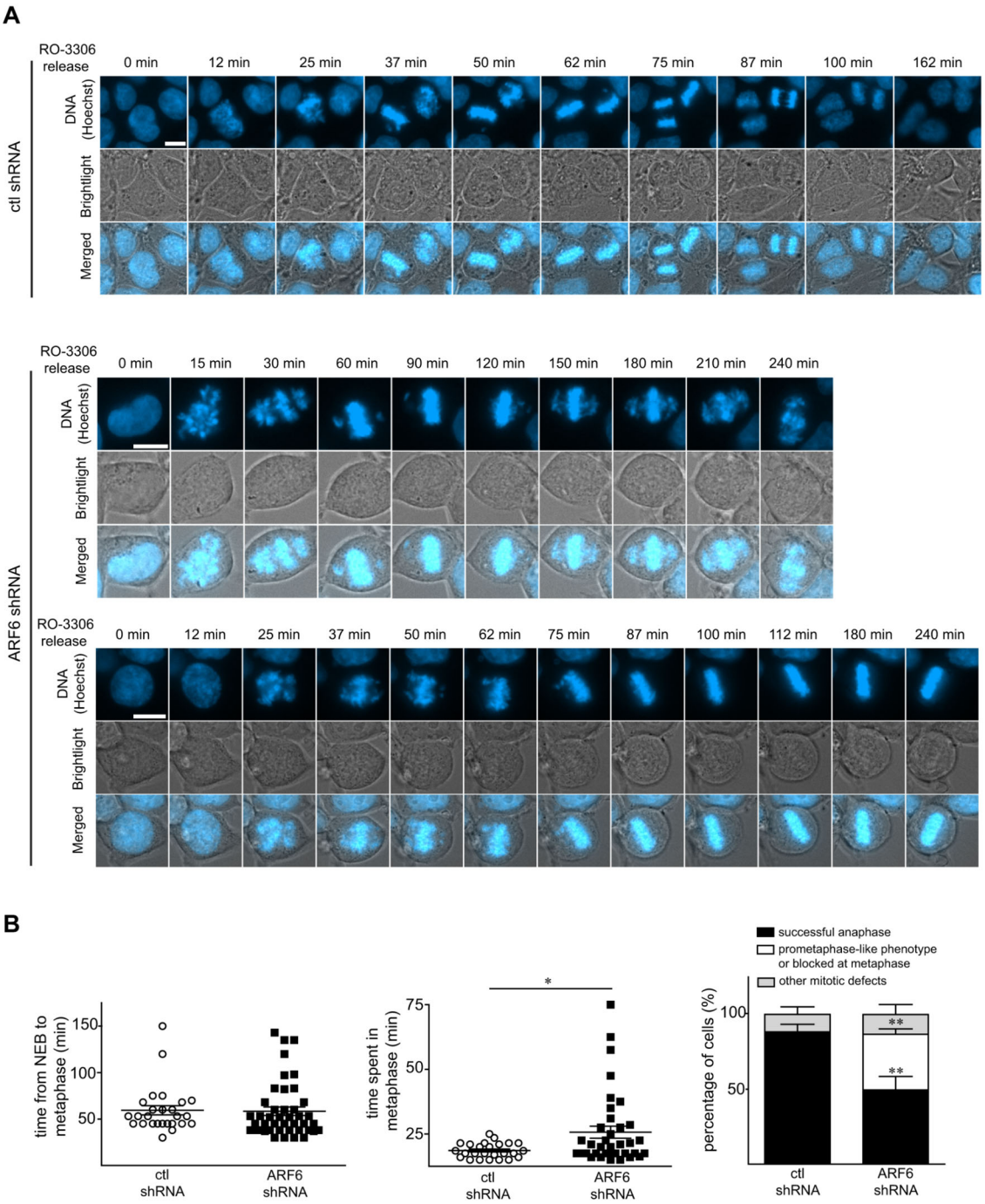


**Fig. 2. ARF6 is essential for the metaphase-anaphase transition.** (A) Control (ctl) and ARF6-depleted cells cultured in complete medium were blocked at the $G_2$/M border, then released by washing out RO3306. Time-lapse imaging was performed and selected images from videos are presented. Note that in ARF6-depleted cells that failed to reach anaphase, chromosomes or chromatids migrated gradually from the metaphase plate to the two poles of the cell to form the prometaphase-like phenotype (top video). In other ARF6-depleted cells, chromosomes remained blocked at the metaphase plate for hours (bottom video). Scale bars: 10 µm. (B) Analysis of mitosis videos obtained using Zeiss Zen imaging software. Time taken from nuclear envelope breakdown (NEB; first visible mitotic event) to form the metaphase plate and time taken from chromosome line up at metaphase to anaphase onset was assessed in analysed videos (27 control cells and 44 ARF6-depleted cells from 4 different experiments) and are presented in the left and the middle graphs, respectively. Error bars represent s.e.m. ($n$=4, $t$-test). We also scored cells that succeeded to reach anaphase, cells that formed the prometaphase-like phenotype or were blocked at metaphase and cells that exhibited other mitotic defects including chromosome congression defect and multipolar spindle (total of 55 control cells and 85 ARF6-depleted cells from 4 different experiments). Results are presented in the graph on the right. Means±s.e.m. of 4 independent experiments are shown ($n$=4, two-way ANOVA). *$P$<0.05, **$P$<0.01.

was degraded in control cells versus only 45% in ARF6-depleted cells. Interestingly, time courses of cyclin B degradation and histone H3 phosphorylation correlated perfectly.

We also performed cell cycle FACS experiments with control and ARF6-depleted cells synchronized by 14 h of RO3306 treatment and released or not for 3 h or 6 h. FACS results were consistent with

Journal of Cell Science (2018) 131, jcs216598. doi:10.1242/jcs.216598

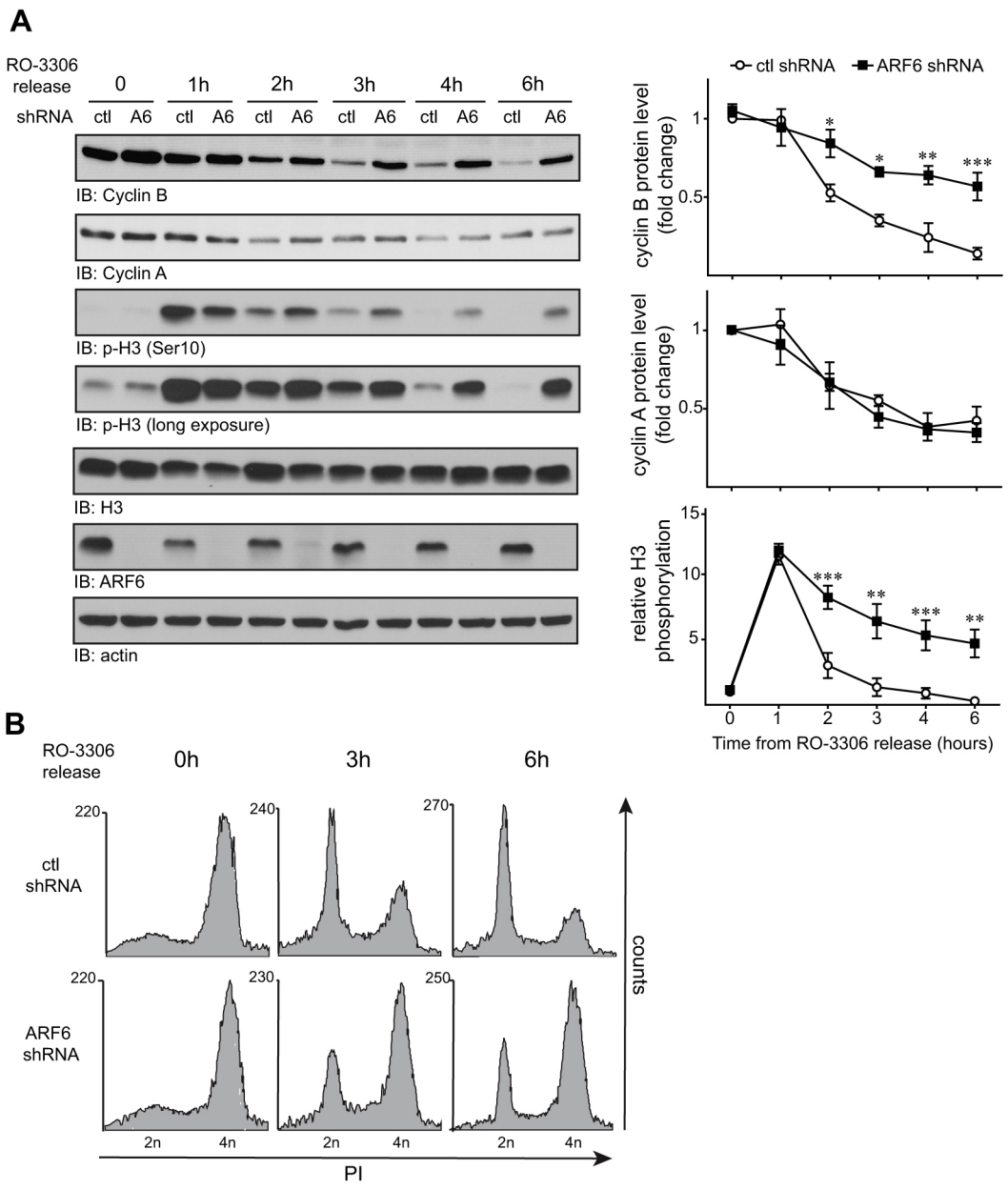


**Fig. 3. Degradation of cyclin B but not cyclin A requires ARF6.** (A) Control (ctl) and ARF6-depleted (A6) cells were synchronized at the $G_2$/M border (14 h RO3306 treatment), released by changing the culture medium and lysed at the indicated times after RO3306 release. Time 0 represents the condition where cells were not released. Cell lysates were subjected to western blot analysis. The graph shows means±s.e.m. of 4 independent experiments ($n$=4, two-way ANOVA). (B) Control (ctl) and ARF6-depleted cells were synchronized at the $G_2$/M border as in A, released or not for 3 h or 6 h, then subjected to cell cycle analysis using FACS. Results presented are representative of three independent experiments ($n$=3). *$P$<0.05, **$P$<0.01, ***$P$<0.001.

live cell and western blot experiments. After RO3306 release, control cells normally exited the $G_2$/M phase and entered the $G_0$/$G_1$ phase, whereas most ARF6-depleted cells remained blocked at the $G_2$/M phase (Fig. 3B).

Given that ARF6 is essential for metaphase/anaphase transition, we asked whether this GTPase becomes active at the metaphase stage to mediate the anaphase onset. We know from live cell experiments that cells reach the metaphase stage 60-75 min after RO3306 release. We therefore measured ARF6 activation in synchronized cells 1 h after RO3306 release. As shown in Fig. S4A, ARF6-GTP levels increased by 90% at metaphase. To explore the significance of this activation, we carried out synchronization/release experiments with control (vector) and dominant-negative T27N-ARF6-overexpressing cells. Overexpression of the T27N-ARF6 mutant did not affect the kinetics of mitotic progression assessed by histone H3 phosphorylation (Fig. S4B). To further investigate the function of ARF6 during mitosis, we aimed to determine its localization using confocal microscopy. We were not able to detect the endogenous protein. So, we overexpressed the HA-tagged wild-type form of ARF6 (HA-ARF6). As illustrated in Fig. S4C, HA-ARF6 was enriched at the membrane during interphase, which corresponds with its normal localization (D'Souza-Schorey et al., 1995), but surprisingly became more diffuse at the cytoplasm during mitosis.

Cyclin B degradation and anaphase onset require SAC satisfaction (Castro et al., 2005). Therefore, we asked whether ARF6 depletion could maintain SAC active, which resulted in the inhibition of cyclin

Journal of Cell Science (2018) 131, jcs216598. doi:10.1242/jcs.216598

B degradation and blockage of cells at metaphase. We assessed the recruitment of BUBR1, a SAC component, to the kinetochores of cells blocked at metaphase (45 min RO3306 release+1 h MG132). In control cells, BUBR1 fluorescence intensity was very low at kinetochores, indicating SAC satisfaction. In contrast, the SAC was maintained active in ARF6-depleted cells, as BUBR1 was enriched at kinetochores of these cells (Fig. 4A). An active SAC could inhibit the E3 ubiquitin ligase APC/$C^{Cdc20}$ responsible for cyclin B ubiquitylation. To confirm this, we evaluated the ubiquitylation state of this cyclin. Cells were synchronized with RO3306 for 14 h then released (1 h release+1 h MG132) and cyclin B was immunoprecipitated. As shown in Fig. 4B, cyclin B ubiquitylation was reduced when ARF6 was knocked down. We also measured the 26S proteasome activity in unsynchronized control and ARF6-depleted cells. As illustrated in Fig. 4C, no significant differences were observed between the two conditions, indicating that ARF6 knockdown does not affect the protein degradation machinery.

### ARF6 is required for the establishment of stable kinetochore-microtubule attachments

To satisfy the SAC, correct and stable kinetochore to microtubule (K-MT) attachments must be established on all chromosomes. We studied these attachments at the metaphase stage (45 min RO3306 release+25 min MG132) in control and ARF6-depleted cells by immunostaining tubulin (microtubules) and CENP-A (known to localize to the inner kinetochore). Microtubules in control cells

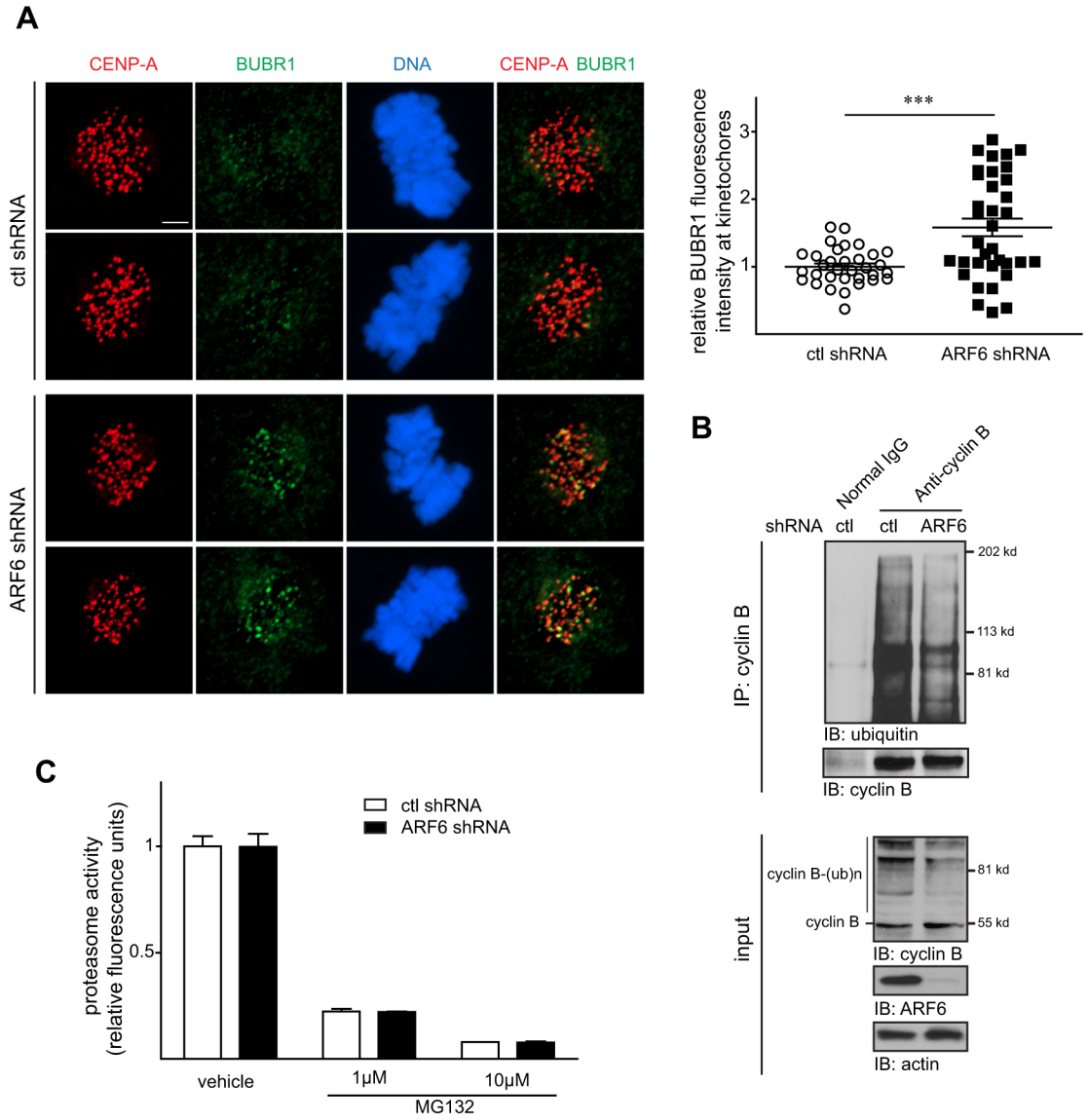


**Fig. 4. ARF6 depletion activates SAC and reduces cyclin B ubiquitylation without affecting proteasome activity.** (A) Control (ctl) and ARF6-depleted cells were blocked at the $G_2$/M border then released for 45 min. MG132 (10 μM) was added for an additional 1 h to block cells at metaphase. Images shown are maximum intensity projections of *z*-stack confocal planes (0.25 μm interval). Scale bar: 2 μm. Quantification of BUBR1 fluorescence intensity in the whole cell (maximum intensity projections) was performed using ImageJ software and results from three different experiments (total of 33 control cells and 35 ARF6-depleted cells) are presented in the graph. Error bars represent s.e.m. (*n*=3, *t*-test). (B) Control (ctl) and ARF6-depleted cells were synchronized and blocked at metaphase as in A. Cells were then harvested and cyclin B immunoprecipitated. Ubiquitylation of this cyclin was assessed by western blot analysis (*n*=3). (C) Unsynchronized control (ctl) and ARF6-depleted cells were treated with DMSO or MG132 (1 μM or 10 μM) for 30 min and proteasome activity was measured. The graph shows means±s.e.m. of 3 independent experiments (*n*=3, two-way ANOVA). ***$P$<0.001.

Journal of Cell Science (2018) 131, jcs216598. doi:10.1242/jcs.216598

formed bi-oriented end-on attachments to kinetochores. These K-fibres (microtubule bundles) were stable as they were thick, well defined and stretched (Fig. 5A, boxes 1 and 2). In contrast, K-fibres in ARF6-depleted conditions were discontinuous, wavy and exhibited a low density of tubulin staining, indicating high instability of the microtubules (Fig. 5A, arrowheads in boxes 3-5). Surprisingly, a large majority of these unstable K-fibres formed bi-oriented end-on (but unstable) interactions with kinetochores (Fig. 5A, arrows in boxes 3-5). Unattached kinetochores and kinetochores with lateral attachments (Fig. 5A, box 6) were also frequently observed in ARF6-depleted cells. To quantify K-fibre stability, we exploited the fact that stable K-fibres contain a large number of microtubule filaments organized in bundles and therefore exhibit higher tubulin density. Thus, using confocal images, we quantified tubulin fluorescence intensity around kinetochores (maximum intensity projections of *z*-stack scan). We drew a box containing all centromeres/kinetochores of the cell and measured the fluorescence intensity of tubulin inside the box. ARF6 depletion resulted in a 40% decrease in tubulin fluorescence intensity around kinetochores, indicating a loss of K-fibre stability.

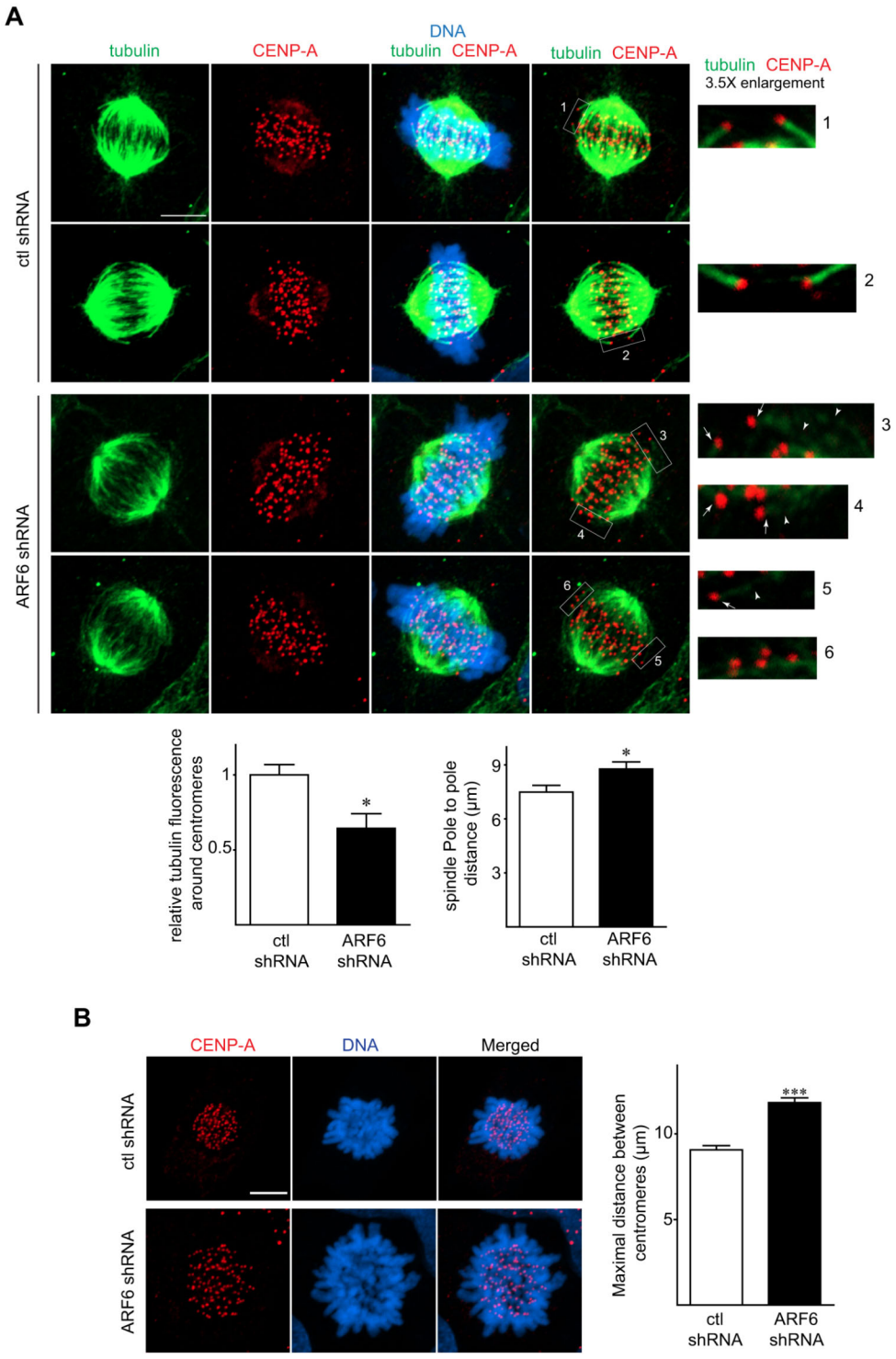


**Fig. 5. ARF6 depletion alters K-fibre stability and chromosome positioning at the metaphase plate.** (A) Control (ctl) and ARF6-depleted cells blocked at metaphase (45 min of RO3306 release followed by 25 min of MG132 exposure) were examined using confocal microscopy. Images of maximum intensity projections of *Z*-stack planes (0.25 µm interval) are presented. Arrows indicate end-on K-MT attachments and arrowheads indicate unstable microtubules. Scale bar: 5 µm. A box containing all centromeres (CENP-A) of the cell was drawn. Fluorescence intensity of tubulin inside the box was quantified using ImageJ. Quantification of tubulin fluorescence intensity in 27 control and 30 ARF6-depleted cells from three different experiments is presented in the left graph. Error bars represent s.e.m. ($n$=3, *t*-test). Mitotic pole to pole distance measured with Zeiss Zen software (27 control cells and 29 ARF6-depleted cells) is shown in the graph on the right. Error bars represent s.e.m. ($n$=3, *t*-test). (B) Cells were treated as in A and images presented are maximum intensity projections of *Z*-stack confocal planes (0.25 µm interval) showing metaphase plates oriented horizontally with respect to the imaging plane. Scale bar: 5 µm. To assess chromosome dispersion, a circle containing all centromeres at the metaphase plate was drawn and circle diameter was measured using Zeiss Zen software. Analysis of 28 control cells and 31 ARF6-depleted cells from three different experiments is presented in the graph. Error bars represent s.e.m. ($n$=3, *t*-test). *$P$<0.05, ***$P$<0.001.

Journal of Cell Science (2018) 131, jcs216598. doi:10.1242/jcs.216598

We also measured the mitotic spindle length and found that the pole to pole distance was 17% longer in ARF6-depleted cells (Fig. 5A). To better understand how chromosomes are positioned at the metaphase plate, we also took images of metaphase plates that were horizontally oriented in respect to the imaging plane (Fig. 5B). We made a *z*-stack scan of cells and using images of maximum intensity projections, we quantified the distance between the furthest centromeres at the metaphase plate by drawing a circle containing all centromeres and measuring the diameter of the circle. Imaging analysis showed that the diameter of centromere circle was significantly bigger (30%) in ARF6-depleted cells than that in control cells, which suggests that chromosomes become more dispersed at the metaphase plate when ARF6 is knocked down, corresponding to the defect in chromosome-microtubule attachments.

### ARF6 protects centromeric sister chromatid cohesion

As illustrated in Fig. S3, we noticed the presence of single chromatids in ARF6-depleted cells that formed the prometaphase-like phenotype. To investigate whether ARF6 plays a role in maintaining sister-chromatid cohesion, we prepared mitotic spreads of control and ARF6-depleted cells at the metaphase stage (55 min after RO3306 release). Based on the degree of cohesion along chromosome arms and at centromeres, we identified three phenotypes: (1) closed arms (tight cohesion at centromeres and along arms); (2) partially open arms (arms are mildly open, but cohesion is maintained tight at centromeres); (3) parallel spaced arms (impaired cohesion at centromeres and along chromosome arms). These phenotypes were scored in control and ARF6-depleted cells from three different experiments. The majority of chromosomes (81%) in control cells displayed closed arms, 15% exhibited partially open arms and only 3% showed parallel spaced arms. Loss of ARF6 substantially impaired sister chromatid cohesion as 62% of cells exhibited parallel spaced arms and only 12% of cells maintained closed arms (Fig. 6A). By analysing the mitotic spreads, we observed that control chromosomes seemed to be more condensed. To quantify this, we measured the length of the longest chromosome in these spreads and found that ARF depletion resulted in a 12% increase in the average length of the longest chromosomes in spreads. To further examine cohesion defects in ARF6-depleted cells, we challenged centromeric cohesion by blocking cells at metaphase for 4 h with MG132 40 min after RO3306 release. Centromeric cohesion resisted the pulling forces of the spindle in control cells (92% of cells); however, ARF6-depleted cells failed to maintain centromeric cohesion and exhibited mitotic spreads with totally scattered chromatids (75% of the cells), indicating a complete loss of sister chromatid cohesion (Fig. 6B). To determine whether microtubules and the spindle are required for the loss of cohesion in ARF6-depleted cells, we incubated cells with the microtubule-depolymerizing agent nocodazole for 4 h after 40 min RO3306 release and performed mitotic spreads. Nocodazole incubation is known to induce the removal of cohesin complex along chromosome arms, but not at centromeres. In our experiments, 95% of control cells maintained centromeric cohesion on all chromosomes versus 45% of ARF6-depleted cells. ARF6 knockdown caused a loss of centromeric cohesion of few chromosomes in 35% of cells and complete chromatid scattering in 25% of the cells (Fig. 6C). Altogether, these results show that ARF6 prevents the premature loss of centromeric cohesion.

### ARF6 depletion enriches PLK1 at microtubules around centromeres

PLK1 is known to phosphorylate the cohesin SA2 subunit causing cohesin dissociation from chromosomes in prometaphase (Sumara et al., 2002; Hauf et al., 2005), except for the centromeric cohesin, which is protected by shugoshin and the phosphatase PP2A until anaphase (Kitajima et al., 2006). To determine whether PLK1 is responsible for the loss of cohesion observed in ARF6-depleted cells, we evaluated the localization of this kinase at metaphase (45 min RO3306 release+25 min MG132). In both conditions (control and ARF6 depletion), PLK1 accumulated at centrosomes. In control cells, PLK1 localized in small amounts at kinetochores (in proximity to CENP-A) (Fig. 7B) as previously reported (Liu et al., 2012). However, ARF6 depletion resulted in an enrichment of PLK1 on microtubules around centromeres (Fig. 7A,B). In 91% of ARF6-depleted cells (versus 22% of control cells), PLK1 formed filaments along microtubules around centromeres/kinetochores suggesting that PLK1 accumulation in proximity of centromeres may cause the impairment of centromeric cohesion in ARF6-depleted cells.

## DISCUSSION

The GTPase ARF6 has previously been shown to play a role in cytokinesis (Makyio et al., 2012; Schweitzer et al., 2005). Here, we demonstrate that ARF6 protects sister chromatid centromeric cohesion until anaphase onset. By maintaining centromeric cohesion, ARF6 promotes the establishment of stable kinetochore-microtubule attachments, SAC satisfaction and the metaphase/anaphase transition. First, we showed, using three different techniques (FACS, western blot and fluorescence microscopy), that ARF6 is important for mitotic progression as depletion of ARF6 blocked cells at mitosis. Analysis of mitotic phenotypes revealed that the increase in mitotic index observed after ARF6 depletion is mainly due to a specific abnormal mitotic phenotype that we called the ‘prometaphase-like’ phenotype (observed in 3% of cells). This phenotype is characterized by the presence of a metaphase plate at the equator with two groups of chromosomes/chromatids positioned symmetrically at the two poles of the cell. The multinucleated cells observed in abundance when ARF6 was depleted are the end products of the prometaphase-like and the multipolar spindle phenotypes as confirmed by live cell microscopy. These multinucleated cells, combined with mitotic cells, could explain the 11% increase in the $G_2$/M population seen in FACS analysis.

Live cell microscopy experiments clearly demonstrate that ARF6 is required for the metaphase/anaphase transition. Although chromosome congression in ARF6-depleted cells was normal and chromosomes took the same time as in control cells to line up at the metaphase plate, the anaphase onset was blocked in nearly half of ARF6-depleted cells. The majority of these cells formed the prometaphase-like phenotype after chromosomes/chromatids scattered gradually from the metaphase plate to the two poles of the cell. The remaining cells were blocked at metaphase for hours (3-4 h). So, the prometaphase-like phenotype seen abundantly in unsynchronized ARF6-depleted cells is a consequence of the metaphase-anaphase transition failure. A similar phenomenon called ‘cohesion fatigue’ was previously reported describing unscheduled chromatid separation in cells delayed at metaphase (Daum et al., 2011; Stevens et al., 2011). In our experiments, both single separated chromatids and complete chromosomes (paired chromatids) scattered to the two poles of the cell from the metaphase plate. Therefore, we conclude that the prometaphase-like phenotype is a result of both chromosome misalignment and a complete loss of cohesion between sister chromatids (cohesion fatigue).

Our findings speculate that ARF6-depleted cells failed to reach anaphase because SAC was not satisfied. In these cells, active SAC inhibited cyclin B ubiquitylation and its degradation, but cyclin A was normally degraded. This is consistent with previous reports

Journal of Cell Science (2018) 131, jcs216598. doi:10.1242/jcs.216598

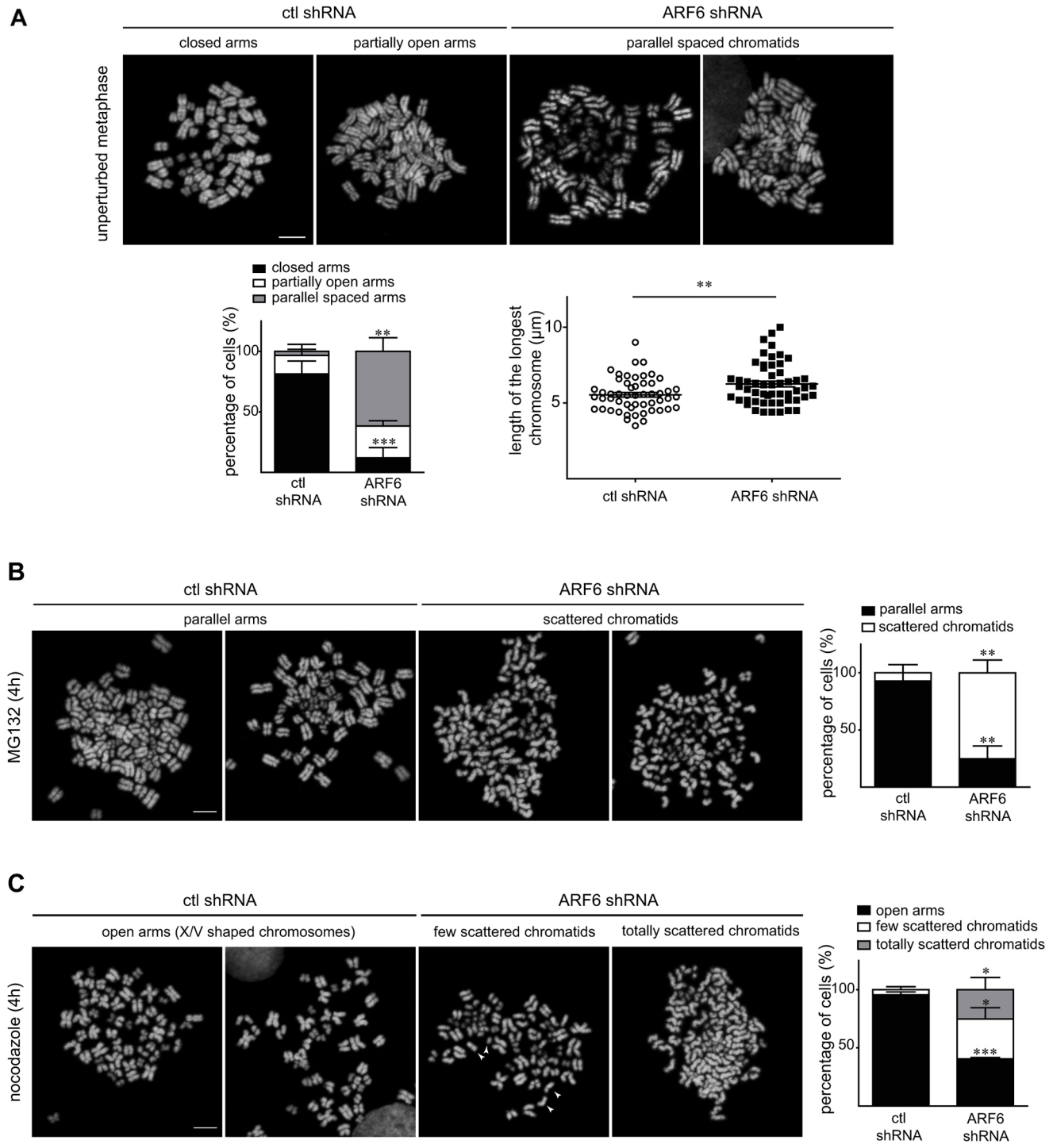


**Fig. 6. ARF6 protects sister chromatid cohesion.** (A) Control (ctl) and ARF6-depleted cells were enriched in metaphase (55 min of RO3306 release) and mitotic spreads examined. Images shown are representative of the three phenotypes found. These phenotypes were scored in spreads from three experiments (total of 64 control and 83 ARF6-depleted cells). Percentage of different phenotypes in each experiment is presented in the graph on the left. Error bars represent s.e.m. ($n$=3, two-way ANOVA). In these spreads, the length of the longest chromosome in each spread was measured and results from 53 control and 54 ARF6-depleted cells are shown in the graph on the right. Error bars represent s.e.m. ($t$-test). (B,C) Control (ctl) and ARF6-depleted cells were synchronized at the $G_2$/M border, released for 40 min and MG132 (10 μM) (B) or nocodazole (1 μM) (C) was added to the medium for an additional 4 h. Spreads were prepared and phenotypes (presented in the images) were scored in three independent experiments (in B, $n$=64 control and $n$=94 ARF6-depleted cells; in C, $n$=60 control and $n$=78 ARF6-depleted cells). Percentages of phenotypes are presented in the graphs. Error bars represent s.e.m. ($n$=3, two-way ANOVA). Scale bars: 5 μm. *$P$<0.05, **$P$<0.01, ***$P$<0.001.

showing that cyclin A degradation occurs early during mitosis, usually before metaphase (den Elzen and Pines, 2001; Geley et al., 2001), whereas cyclin B degradation takes place at the end of metaphase and is associated with anaphase onset (Chang et al., 2003). Interestingly, our results correlate perfectly as, in our experiments, SAC was active in 50% of ARF6-depleted cells, which

Journal of Cell Science (2018) 131, jcs216598. doi:10.1242/jcs.216598

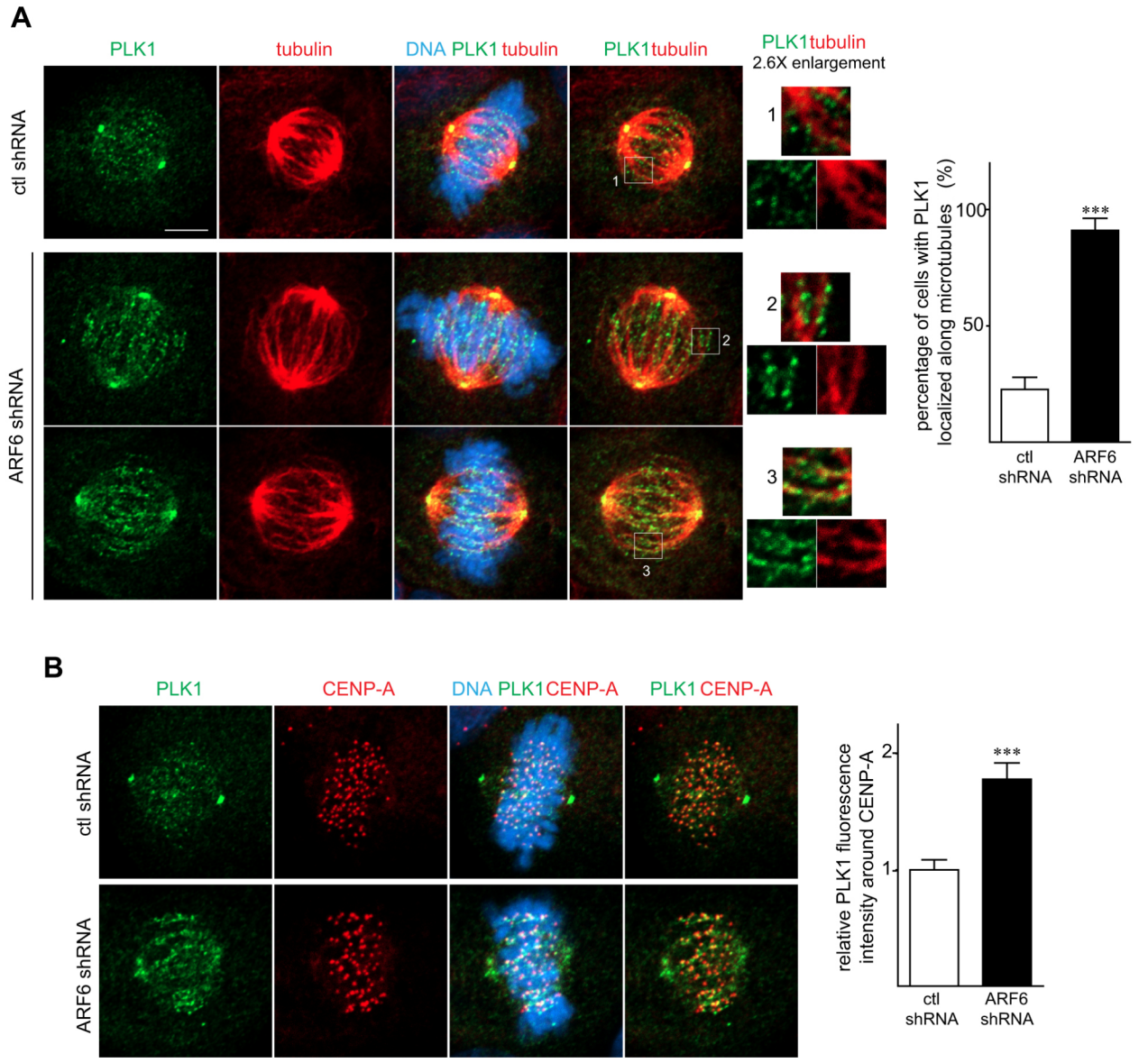


**Fig. 7. ARF6 depletion enriches PLK1 on microtubules around centromeres at metaphase.** (A,B) Control (ctl) and ARF6-depleted cells were blocked at metaphase (45 min of RO3306 release followed by 25 min of MG132). Cells were then fixed and subjected to immunofluorescence staining. *Z*-stack confocal images (0.3 µm interval) were taken and all images presented in the figure are maximum intensity projections of three confocal planes (0.3 µm interval). Scale bar: 5 µm. Cells displaying PLK1 enrichment along microtubules (PLK1 forms filaments as showed in boxes 2 and 3) were scored in four different experiments (total of 42 control and 34 ARF6-depleted cells) and results are presented (mean±s.e.m.) in the graph in A ($n$=4, $t$-test). To quantify PLK1 enrichment around centromeres, small boxes (1 µm×1 µm) containing CENP-A were drawn. Fluorescence intensity of PLK1 inside boxes was quantified in 20 control cells (296 kinetochores) and 22 ARF6-depleted cells (374 kinetochores) from three different experiments using ImageJ software. Quantification of relative PLK fluorescence intensity is presented in the graph in B. Error bars represent s.e.m. ($n$=3, $t$-test). ***$P$<0.001.

explains why nearly half of these cells failed to reach anaphase and justifies why 50% of cyclin B was not degraded.

SAC satisfaction requires the establishment of correct K-MT attachments on all chromosomes (Musacchio and Salmon, 2007; Pesin and Orr-Weaver, 2008). We provide evidence that ARF6 depletion alters the formation and the stability of these attachments maintaining the SAC active. The establishment of stable K-MT attachments is a two-step process. First, end-on bi-oriented attachments are formed usually by conversion of lateral attachments at the metaphase plate (Shrestha and Draviam, 2013; Cai et al., 2009; Magidson et al., 2011). Then, these attachments are stabilized by increasing the number of microtubule bundles bound to sister kinetochores (King and Nicklas, 2000). The widely accepted model suggests that bi-orientation creates a centromeric tension and spatially separates Aurora B (located at the inner centromere) from its substrates at the outer kinetochore, allowing the stabilization of these attachments (Cimini et al., 2006; Liu et al., 2009). Centromeric cohesin has a central role in generating this tension because it counteracts the pulling force of the spindle microtubules (Tanaka et al., 2000). Moreover, our results demonstrate that ARF6 plays a crucial role in maintaining centromeric cohesion of sister chromatids as ARF6 depletion resulted in the impairment of this process. Therefore, we assume that the defect in the establishment of stable K-MT attachments after ARF6 depletion is a direct consequence of a weak centromeric cohesion.

Journal of Cell Science (2018) 131, jcs216598. doi:10.1242/jcs.216598

Although a vast majority of kinetochores observed in ARF6-depleted cells were able to form end-on bi-oriented attachments to microtubules, these K-fibres (microtubules) were very unstable as they were discontinuous and wavy, and exhibited a low density of tubulin, suggesting that centromeric cohesion is needed more for the stabilization of correct K-MT attachments rather than for their initial formation. However, kinetochores with lateral attachments were also frequent (compared with control cells), indicating that the formation of end-on attachments could also depend on intact centromeric cohesion. Because ARF6 depletion alters K-MT attachments, chromosomes were more dispersed at the metaphase plate.

Although ARF6 depletion disturbed K-MT attachment stability, chromosome congression occurred normally in these cells. This coordinates with previous reports showing that chromosome alignment can take place in the absence of stable K-fibres and bi-orientation is established at the spindle equator when lateral attachments are converted to end-on attachments (Cai et al., 2009; Magidson et al., 2011).

Our data show clearly that ARF6 protects sister chromatid cohesion. In unperturbed mitosis, at metaphase, chromosomes in ARF6-depleted cells exhibited parallel spaced arms (a rare phenotype in control cells), suggesting a reduced, but not complete loss of cohesion at the arms and centromeres. However, when challenged with the spindle microtubule pulling forces (MG132 for 4 h), centromeric cohesion totally broke down in 75% of the cells. In ARF6-depleted cells, the spindle microtubule forces aggravated the loss of sister chromatid cohesion, but this event could occur, even if to a lesser degree, in the absence of microtubules (nocodazole for 4 h).

We propose that the degree of cohesion loss in ARF6-depleted cells determines the fate of the cell during mitosis. If the cohesion loss is mild, cells can establish end-on bi-oriented, but unstable K-MT attachments. This lack of tension attachment is sufficient to satisfy the SAC, as previously reported (Etemad et al., 2015). After a delay at metaphase, SAC is satisfied and cells enter anaphase, but because K-fibres are less stable, multiple defects occur, including lagging chromosomes and formation of a bi/multi-lobed nucleus. However, if the cohesion loss is more severe, erroneous K-MT attachments become predominant because of the high microtubule-destabilizing activity due to the severe lack of tension. As a result, SAC remains active and cells are blocked at the metaphase stage. Failing to establish correct attachments at the metaphase plate, chromosomes and separated chromatids scatter gradually to the two poles and form the prometaphase-like phenotype. Decondensation of chromosomes results in the formation of multinucleated cells.

It is clear that sister chromatid cohesion is weakened after ARF6 depletion, but how does this happen? The majority of the cohesin complex is removed from chromosome arms during early phases of mitosis via two main mitotic kinases, PLK1 (Sumara et al., 2002) and Aurora B (Giménez-Abián et al., 2004). Centromeric cohesin is, however, protected by the shugoshin-PP2A (B56α) complex until late metaphase (Kitajima et al., 2006). Indeed, PLK1 phosphorylates the cohesin subunit SA2 causing cohesin dissolution (Hauf et al., 2005), but at centromeres this phosphorylation is counteracted by the protein phosphatase PP2A (B56α). ARF6 may therefore protect centromeric cohesion by facilitating the recruitment of the shugoshin-PP2A complex or restricting the access of PLK1 to centromeres. In our study, we were not able to determine whether recruitment of PP2A was affected by ARF6 depletion as we failed to detect endogenous B56α in immunofluorescence experiments. However, our results indicate that ARF6 depletion enriches PLK1 at microtubules around centromeres. PLK1 formed filaments localized along microtubules near centromeres, suggesting that PLK1 enrichment in the proximity of centromeres may bypass the protection of centromeric SA2 from phosphorylation and cause the loss of cohesion observed in ARF6-depleted cells. In non-dividing cells, ARF6 localizes at the plasma membrane where it controls endocytosis (D'Souza-Schorey et al., 1995). Our data show that, during mitosis, ARF6 is activated and becomes diffuse throughout the cytoplasm. Although the GTPase ARF6 is essential for early phases of mitosis, its GTP-bound form seems to be less necessary at these stages and may be more important later for cytokinesis, as previously reported (Schweitzer and D'Souza-Schorey, 2002). This is not the first time a protein involved in endocytosis has been revealed to be important for mitosis; clathrin and dynamin, for example, do not seem to be connected to membranes during mitosis but they bind partners that are distinct from those implicated in internalization (Royle et al., 2005; Thompson et al., 2004). More work is needed to determine the mechanism by which ARF6 regulates the localization of PLK1 to maintain sister chromatid cohesion. Interestingly, GIT1, an ARF6 GTPase-activating protein, has been shown to promote the activation of PAK1 (P21-activated kinase) (Zhao et al., 2005), which phosphorylates PLK1 during mitosis (Maroto et al., 2008). Moreover, a recent study has reported that GIT1 is a substrate of PLK1 at the centromere (Lera et al., 2016). So, GIT1 may form the link between ARF6 and PLK1. Altogether, our findings describe a new function for the GTPase ARF6 in mitosis. This molecular switch provides protection to centromeric cohesion, enabling the formation of stable kinetochore-microtubule attachments and faithful chromosome segregation.

## MATERIALS AND METHODS

### Reagents, antibodies, shRNAs and DNA plasmids

Hoechst 33342 was purchased from Invitrogen (Burlington, ON, Canada). RO3306 and propidium iodide (PI) were from Sigma-Aldrich (Oakville, ON, Canada). Puromycin was from Invivogen (San Diego, CA, USA) and MG132 from MedChem Express (Monmouth Junction, NJ, USA). Antibodies against phospho-Histone H3 (Ser10) (#3377, 1:5000), Histone H3 (#9715, 1:5000), cyclin B1 (#4138, 1:5000), cyclin A2 (#4656, 1:5000), pan-actin (#4968, 1:5000), ubiquitin (#3936, 1:5000) and PLK1 (#4513, 1:200) were from Cell Signaling (Danvers, MA, USA). Anti-ARF6 (#sc-7971, 1:1000) was from Santa Cruz Biotech (Santa Cruz, CA, USA). Anti-CENP-A (#ab13939, 1:200) and anti-HA tag (#ab16918, 1/200) were from Abcam (Toronto, ON, Canada). Anti-BUBR1 (#A300-386A, 1:200) was purchased from Bethyl laboratories (Montgomery, TX, USA). Anti-α-tubulin (#14555-1-AP, 1:200) was from Proteintech (Rosement, IL, USA). Goat anti-mouse and goat anti-rabbit horseradish peroxidase-conjugated antibodies (#HAF007 and #HAF008, 1:10000) were from R&D Systems (Minneapolis, MN, USA). ARF6 shRNA and scrambled shRNA lentiviral plasmids (pLKO.1-puro) were provided as bacterial glycerol stocks by Sigma and lentiviruses were then produced in HEK293T cells. The sequence of shARF6 is found in the MISSION shRNA Library, Sigma (ARF6 shRNA, Clone ID: NM_001663.3-926s21c1, sequence: ACCGG-AGCTGCACCGCATTATCAATGCTCGAGCATTGATAATGCGGTGC-AGCTTTTTTTG). shRNA-resistant WT-ARF6 gene cloned in pcDNA3.3-TOPO was synthesized by Invitrogen GeneArt Gene Synthesis (Thermo Fisher, Haverhill, MA, USA).

### Cell culture and lentiviral transduction

HEK293 cells were cultured in EMEM supplemented with 10% fetal bovine serum and penicillin-streptomycin (Wisent, QC, Canada) and incubated at 37°C in a humidified atmosphere (95% air, 5% $CO_2$). To deplete ARF6, the minimal lentivirus concentration that induced maximal knockdown (95-100%) was first determined and used subsequently. For experiments, cells were infected with control (ctl) or ARF6 shRNA lentiviruses and medium was changed after 8 h. Cells were reseeded after 48 h and used at day 4 after lentiviral infection. In fluorescence live cell and confocal microscopy experiments, cells were subjected to puromycin selection (10 µg/ml) at day 2 after lentiviral infection before they were used in experiments (day 4). For

Journal of Cell Science (2018) 131, jcs216598. doi:10.1242/jcs.216598

cell synchronization at $G_2$/M border, cultured cells (day 3 after lentiviral infection) were treated with the specific CDK1 inhibitor RO3306 (9 µM) for 14 h, then released by washing out RO3306.

### Western blotting

Cells were lysed in lysis buffer (50 mM Tris-HCl, 1% NP-40, 10% glycerol, 140 mM NaCl, 5 mM $MgCl_2$, 20 mM NaF, 1 mM NaPPi and 1 mM orthovanadate, pH 7.4) complemented with protease inhibitors: aprotinin (5 µg/ml), benzamidine (150 µg/ml), leupeptin (5 µg/ml), pepstatin (4 µg/ml) and phenylmethylsulfonyl fluoride (1 mM). Total soluble proteins were then denatured, run on polyacrylamide gels and transferred onto nitrocellulose membranes. After BSA blocking, membranes were incubated with specific primary antibodies overnight. Horseradish peroxidase-conjugated secondary antibodies were then added and proteins were detected by chemiluminescence (ECL Prime, GE Healthcare, Mississauga, ON, Canada). The digital images obtained were quantified using ImageJ software.

### GST pull-down assay

To measure ARF6 activation levels, we carried out GST pull-down assays. Briefly, cells were lysed in the same lysis buffer used for western blot and total soluble proteins were incubated on a rotator with GST-GGA3-glutathione-Sepharose 4B beads for 1 h at 4°C. ARF6-GTP bound to beads was then eluted, run on polyacrylamide gel and quantified using western blot.

### Immunoprecipitation

To immunoprecipitate proteins, cells were lysed in TGH buffer (50 mM HEPES, pH 7.3, 1% Triton X-100, 10% glycerol, 50 mM NaCl, 5 mM EDTA) supplemented with protease inhibitors: aprotinin (5 µg/ml), benzamidine (150 µg/ml), leupeptin (5 µg/ml), pepstatin (4 µg/ml) and phenylmethylsulfonyl fluoride (1 mM) and the phosphatase inhibitor orthovanadate (1 mM). In each condition, 700 µg total lysate was incubated with 2 µg of the specific antibody overnight at 4°C in a rotator, then 40 µl of prewashed protein A/G plus Agarose beads were added and the sample was re-incubated for 2 h at 4°C in a rotator. After three washes, precipitated proteins were eluted and detected using western blot.

### Cell cycle, cell size and proliferation

For cell cycle analysis, cells were trypsinized, washed in PBS and fixed with ice-cold ethanol (80%) dropwise while vortexing. Cells were kept in ethanol overnight at 4°C, then washed with PBS, permeabilized with 0.2% Triton X-100 for 15 min and washed again. After incubation for 1 h with RNase A (10 µg/ml), DNA was labelled with 50 µg/ml PI and cells were analysed using FACS. Quantification of cell cycle populations was obtained using ModFit LT software. For cell size determination, cells were trypsinized, washed and resuspended in PBS, then subjected to FACS analysis based on forward scatter/side scatter (FS/SSC). For proliferation assay, equal numbers (1 million) of control and ARF6-depleted cells (day 3 from lentiviral infection) were seeded to grow in complete medium (EMEM +10% FBS) then manually counted using a haemocytometer after 2 days in culture.

### Proteasome activity

The chymotrypsin-like activity of the 26S proteasome was measured as described previously (Kisselev and Goldberg, 2005). Cells were harvested in proteasome activity assay buffer (50 mM Tris-HCl, pH 7.5, 250 mM sucrose, 5 mM $MgCl_2$, 0.5 mM EDTA, 1 mM dithiothreitol) and lysed by passing 15 times through a 27-gauge needle attached to a 1 ml syringe. Lysates were centrifuged at 10,000 ***g*** for 10 min at 4°C and concentration of total proteins in supernatants was determined using the BCA protein assay (Thermo Fisher Scientific, MA, USA). 50 µg of proteins per well were transferred to a black 96-well plate with clear bottom (Corning, NY, USA) and incubated with 100 µM of the fluorogenic substrate, Suc-Leu-Leu-Val-Tyr-AMC (Enzo Life Sciences., Inc., NY, USA) for 1 h at 37°C. Fluorescence (380 nm excitation, 460 nm emission) was measured with SpectraMax M2 microplate reader (Molecular Devices Corporation, Sunnyvale, CA, USA). Fluorescence values were corrected by subtracting the blank value (fluorogenic substrate in buffer without lysate) and the mean of triplicates of each condition was considered.

### Fluorescence, live cell and confocal microscopy

For fluorescence microscopy, cells were grown on 24-well plate (Corning, NY, USA) or glass-bottom culture dish (Mat Tek Corporation, MA, USA) coated with 0.1% gelatin. Cells were then fixed with 4% formaldehyde solution and DNA was stained with 3 µg/ml Hoechst 33342 for 10 min. Cells were washed and maintained in PBS. Images were then immediately captured using a Zeiss fluorescence microscope (Carl Zeiss, Germany) equipped with an AxioCam MRm camera (Carl Zeiss) and Zeiss Zen software using 20× or 40× objective.

To perform live cell experiments, cells were grown on 24-well plates (Corning) or glass-bottom culture dishes (Mat Tek) coated with 0.1% gelatin and synchronized with a 6-8 h RO3306 treatment. Hoechst 33342 (1 µg/ml) was added to the culture medium 10 min before releasing cells by washing out RO3306 (changing the culture medium). Plates or culture dishes were rapidly placed in the 37°C heated chamber (5% $CO_2$) and images were captured every 7.5 to 30 min over 2-6 h (10 ms exposure time with the minimum intensity of the fluorescence lamp) using the 20× objective for the 24-well plate and the 40× objective for the glass-bottom culture dish. Live cell videos were obtained and processed with Zeiss Zen imaging software.

For confocal microscopy, cells were grown on glass coverslips coated with 0.1% gelatin, synchronized at the $G_2$/M border with RO3306 (4 h to 14 h incubation), released by changing the culture medium, then fixed with a 4% formaldehyde solution. After 1 h of blocking and permeabilization with 1.5% BSA solution containing 0.05% saponin, coverslips were incubated with the primary antibodies in blocking solution (1:200) for 90 min, washed twice with PBS and incubated with secondary antibodies coupled with Alexa Fluor-488/568/633 (Invitrogen, Burlington, ON, Canada) at 1:200 concentration for 90 min. DNA was stained with Hoechst 33342 (3 µg/ml) for 10 min before mounting coverslips with Aqua-Mount (Lerner Laboratories). Images were captured using Zeiss confocal microscope LSM800 controlled by Zeiss Zen imaging software. The same software was used for quantification of distances and ImageJ was used to quantify fluorescence intensities.

### Mitotic spreads

Cells were collected by trypsinization, washed with PBS and incubated with hypotonic buffer (75 mM KCl) for 15 min at 37°C. After centrifugation, the hypotonic buffer was discarded except for a small volume (300 µl). Cells were resuspended in the remaining volume then fixed with ice-cold fixative (3:1 methanol:glacial acetic acid) drop by drop while vortexing. After 1 h on ice, fixative was changed twice and mitotic spreads were prepared by dropping the fixed swollen cells onto glass microscope slides (3 to 4 drops per slide from 10 cm height). The slides were left to dry at room temperature (1-2 h). 1 µl Hoechst 33342 (0.2 mg/ml) was added to one drop of Aqua-Mount (Lerner Laboratories, Pittsburgh, PA, USA) on the slide before mounting the coverslip. Chromosomes were visualized using the same confocal microscope described above.

### Statistical analysis

Statistical analysis was performed using two-tailed *t*-test, one-way or two-way ANOVA analysis of variance followed by a Bonferroni's multiple comparison test using GraphPad Prism (version 5, San Diego, CA, USA) as indicated in the figure legends.

#### Acknowledgements

We thank Gilles Hickson and Sebastien Carreno for comments and critical reading of the manuscript.

#### Competing interests

The authors declare no competing or financial interests.

#### Author contributions

Conceptualization: M.B., A.C.; Methodology: M.B., R.C.; Validation: M.B.; Formal analysis: M.B., A.C.; Investigation: R.C.; Writing - original draft: M.B.; Writing - review & editing: A.C.; Supervision: A.C.; Project administration: A.C.; Funding acquisition: A.C.

#### Funding

This work was supported by the Canadian Institutes of Health Research (CIHR) to A.C.

**Supplementary information**

Supplementary information available online at
http://jcs.biologists.org/lookup/doi/10.1242/jcs.216598.supplemental

**References**


**Boshans, R. L., Szanto, S., Van Aelst, L. and D'souza-Schorey, C.** (2000). ADP-ribosylation factor 6 regulates actin cytoskeleton remodeling in coordination with Rac1 and RhoA. *Mol. Cell. Biol.* **20**, 3685-3694.

**Bourmoum, M., Charles, R. and Claing, A.** (2016). The GTPase ARF6 controls ROS production to mediate angiotensin II-induced vascular smooth muscle cell proliferation. *PLoS ONE* **11**, e0148097.

**Cai, S., O'connell, C. B., Khodjakov, A. and Walczak, C. E.** (2009). Chromosome congression in the absence of kinetochore fibres. *Nat. Cell Biol.* **11**, 832-838.

**Castro, A., Bernis, C., Vigneron, S., Labbé, J.-C. and Lorca, T.** (2005). The anaphase-promoting complex: a key factor in the regulation of cell cycle. *Oncogene* **24**, 314.

**Chang, D. C., Xu, N. and Luo, K. Q.** (2003). Degradation of Cyclin B is required for the onset of anaphase in mammalian cells. *J. Biol. Chem.* **278**, 37865-37873.

**Cimini, D., Wan, X., Hirel, C. B. and Salmon, E. D.** (2006). Aurora kinase promotes turnover of kinetochore microtubules to reduce chromosome segregation errors. *Curr. Biol.* **16**, 1711-1718.

**Daum, J. R., Potapova, T. A., Sivakumar, S., Daniel, J. J., Flynn, J. N., Rankin, S. and Gorbsky, G. J.** (2011). Cohesion fatigue induces chromatid separation in cells delayed at metaphase. *Curr. Biol.* **21**, 1018-1024.

**den Elzen, N. and Pines, J.** (2001). Cyclin a is destroyed in prometaphase and can delay chromosome alignment and anaphase. *J. Cell Biol.* **153**, 121-136.

**D'souza-Schorey, C., Li, G., Colombo, M. I. and Stahl, P. D.** (1995). A regulatory role for ARF6 in receptor-mediated endocytosis. *Science* **267**, 1175-1178.

**D'souza-Schorey, C., Van Donselaar, E., Hsu, V. W., Yang, C., Stahl, P. D. and Peters, P. J.** (1998). ARF6 targets recycling vesicles to the plasma membrane: insights from an ultrastructural investigation. *J. Cell Biol.* **140**, 603-616.

**Etemad, B., Kuijt, T. E. F. and Kops, G. J. P. L.** (2015). Kinetochore–microtubule attachment is sufficient to satisfy the human spindle assembly checkpoint. *Nat. Commun.* **6**, 8987.

**Geley, S., Kramer, E., Gieffers, C., Gannon, J., Peters, J.-M. and Hunt, T.** (2001). Anaphase-promoting complex/cyclosome–dependent proteolysis of human cyclin a starts at the beginning of mitosis and is not subject to the spindle assembly checkpoint. *J. Cell Biol.* **153**, 137-148.

**Giménez-Abián, J. F., Sumara, I., Hirota, T., Hauf, S., Gerlich, D., De La Torre, C., Ellenberg, J. and Peters, J.-M.** (2004). Regulation of sister chromatid cohesion between chromosome arms. *Curr. Biol.* **14**, 1187-1193.

**Godek, K. M., Kabeche, L. and Compton, D. A.** (2015). Regulation of kinetochore-microtubule attachments through homeostatic control during mitosis. *Nat. Rev. Mol. Cell Biol.* **16**, 57-64.

**Hauf, S., Roitinger, E., Koch, B., Dittrich, C. M., Mechtler, K. and Peters, J. M.** (2005). Dissociation of cohesin from chromosome arms and loss of arm cohesion during early mitosis depends on phosphorylation of SA2. *PLoS Biol.* **3**, e69.

**Hood, E. A., Kettenbach, A. N., Gerber, S. A. and Compton, D. A.** (2012). Plk1 regulates the kinesin-13 protein Kif2b to promote faithful chromosome segregation. *Mol. Biol. Cell* **23**, 2264-2274.

**King, J. M. and Nicklas, R. B.** (2000). Tension on chromosomes increases the number of kinetochore microtubules but only within limits. *J. Cell Sci.* **113**, 3815-3823.

**Kisselev, A. F. and Goldberg, A. L.** (2005). Monitoring activity and inhibition of 26S proteasomes with fluorogenic peptide substrates. *Methods Enzymol.* **398**, 364-378.

**Kitajima, T. S., Sakuno, T., Ishiguro, K.-I., Iemura, S.-I., Natsume, T., Kawashima, S. A. and Watanabe, Y.** (2006). Shugoshin collaborates with protein phosphatase 2A to protect cohesin. *Nature* **441**, 46.

**Lera, R. F., Potts, G. K., Suzuki, A., Johnson, J. M., Salmon, E. D., Coon, J. J. and Burkard, M. E.** (2016). Decoding Polo-like kinase 1 signaling along the kinetochore–centromere axis. *Nat. Chem. Biol.* **12**, 411.

**Liu, D., Vader, G., Vromans, M. J. M., Lampson, M. A. and Lens, S. M.** (2009). Sensing chromosome bi-orientation by spatial separation of aurora B kinase from kinetochore substrates. *Science* **323**, 1350-1353.

**Liu, D., Davydenko, O. and Lampson, M. A.** (2012). Polo-like kinase-1 regulates kinetochore–microtubule dynamics and spindle checkpoint silencing. *J. Cell Biol.* **198**, 491-499.

**Magidson, V., O'connell, C. B., Loncarek, J., Paul, R., Mogilner, A. and Khodjakov, A.** (2011). The spatial arrangement of chromosomes during prometaphase facilitates spindle assembly. *Cell* **146**, 555-567.

**Makyio, H., Ohgi, M., Takei, T., Takahashi, S., Takatsu, H., Katoh, Y., Hanai, A., Ueda, T., Kanaho, Y., Xie, Y. et al.** (2012). Structural basis for Arf6–MKLP1 complex formation on the Flemming body responsible for cytokinesis. *EMBO J.* **31**, 2590-2603.

**Maroto, B., Ye, M. B., Von Lohneysen, K., Schnelzer, A. and Knaus, U. G.** (2008). P21-activated kinase is required for mitotic progression and regulates Plk1. *Oncogene* **27**, 4900.

**Murray, A. W., Solomon, M. J. and Kirschner, M. W.** (1989). The role of cyclin synthesis and degradation in the control of maturation promoting factor activity. *Nature* **339**, 280.

**Musacchio, A. and Salmon, E. D.** (2007). The spindle-assembly checkpoint in space and time. *Nat. Rev. Mol. Cell Biol.* **8**, 379-393.

**Pesin, J. A. and Orr-Weaver, T. L.** (2008). Regulation of APC/C activators in mitosis and meiosis. *Annu. Rev. Cell Dev. Biol.* **24**, 475-499.

**Radhakrishna, H., Klausner, R. D. and Donaldson, J. G.** (1996). Aluminum fluoride stimulates surface protrusions in cells overexpressing the ARF6 GTPase. *J. Cell Biol.* **134**, 935-947.

**Royle, S. J., Bright, N. A. and Lagnado, L.** (2005). Clathrin is required for the function of the mitotic spindle. *Nature* **434**, 1152-1157.

**Schweitzer, J. K. and D'souza-Schorey, C.** (2002). Localization and Activation of the ARF6 GTPase during cleavage furrow ingression and cytokinesis. *J. Biol. Chem.* **277**, 27210-27216.

**Schweitzer, J. K., Burke, E. E., Goodson, H. V. and D'souza-Schorey, C.** (2005). Endocytosis resumes during late mitosis and is required for cytokinesis. *J. Biol. Chem.* **280**, 41628-41635.

**Shrestha, R. L. and Draviam, V. M.** (2013). Lateral to end-on conversion of chromosome-microtubule attachment requires kinesins CENP-E and MCAK. *Curr. Biol.* **23**, 1514-1526.

**Stevens, D., Gassmann, R., Oegema, K. and Desai, A.** (2011). Uncoordinated loss of chromatid cohesion is a common outcome of extended metaphase arrest. *PLoS ONE* **6**, e22969.

**Sumara, I., Vorlaufer, E., Stukenberg, P. T., Kelm, O., Redemann, N., Nigg, E. A. and Peters, J.-M.** (2002). The dissociation of cohesin from chromosomes in prophase is regulated by polo-like kinase. *Mol. Cell* **9**, 515-525.

**Tanaka, T., Fuchs, J., Loidl, J. and Nasmyth, K.** (2000). Cohesin ensures bipolar attachment of microtubules to sister centromeres and resists their precocious separation. *Nat. Cell Biol.* **2**, 492.

**Thompson, H. M., Cao, H., Chen, J., Euteneuer, U. and Mcniven, M. A.** (2004). Dynamin 2 binds gamma-tubulin and participates in centrosome cohesion. *Nat. Cell Biol.* **6**, 335-342.

**Uhlmann, F. and Nasmyth, K.** (1998). Cohesion between sister chromatids must be established during DNA replication. *Curr. Biol.* **8**, 1095-1102.

**Waizenegger, I. C., Hauf, S., Meinke, A. and Peters, J.-M.** (2000). Two distinct pathways remove mammalian cohesin from chromosome arms in prophase and from centromeres in anaphase. *Cell* **103**, 399-410.

**Zhao, Z. S., Lim, J. P., Ng, Y. W., Lim, L. and Manser, E.** (2005). The GIT-associated kinase PAK targets to the centrosome and regulates Aurora-A. *Mol. Cell* **20**, 237-249.